Mon. Not. R. Astron. Soc. **000**, 1–?? (2010) Printed 27 December 2010 (MN LATEX style file v2.2)

Mini radio lobes in AGNs core illumination and their hadronic γ-ray afterlight

Motoki Kino[1] and Katsuaki Asano[2]
[1] *National Astronomical Observatory of Japan, 181-8588 Mitaka, Japan*
[2] *Interactive Research Center for Science, Tokyo Institute of Technology, 2-12-1 Ookayama, Tokyo 152-8550, Japan*

ABSTRACT

Recent radio observations reveal the existence of mini radio lobes in active galaxies with their scales of ~ 10 pc. The lobes are expected to be filled with shock accelerated electrons and protons. In this work, we examine the photon spectra from the mini lobes, properly taking the hadronic processes into account. We find that the resultant broadband spectra contain the two distinct hadronic bumps in γ-ray bands, i.e., the proton synchrotron bump at $\sim$ MeV and the synchrotron bump at $\sim$ GeV due to the secondary electrons/positrons produced via photo-pion cascade. Especially when the duration of particle injection is shorter than the lobe age, radio-dark γ-ray lobes are predicted. The existence of the γ-ray lobes could be testable with the future TeV-γ telescope *CTA*.

Key words: jets—galaxies: active—galaxies: gamma-rays—theory

1 INTRODUCTION

Thanks to the progress of VLBI (Very Long Baseline Interferometry) observations, compact radio lobes with a linear size $LS \sim 1$ kpc, defined as a projected length from the core to the lobe, have been discovered (e.g., Fanti et al. 1995; Readhead et al. 1996; O'Dea & Baum 1997). Further VLBI observations recently reveal the existence of very small radio lobes with $LS \sim 10$ pc among two samples of compact radio sources. The sample of compact radio sources with their spectral peaks higher than ~ 5 GHz is termed as high frequency peakers (HFPs). Some of them turn out to be mini lobes based on their morphologies and non-variabilities (e.g., Orienti et al. 2007; Orienti & Dallacasa 2008). The sample of compact radio sources at low-redshift ($z < 0.16$) is selected and called as CORALZ. The VLBI observations of CORALZ show that some of them are also found as mini radio lobes (Snellen et al. 2004; de Vries et al. 2009). Apart from the above two cases, recurrent radio sources are also known to possess mini lobes inside large lobes (e.g., 3C 84, Walker et al. 2000). These mini radio lobes are young and their ages are typically estimated as $t_{\rm age} \sim 10^{2-3}$ yrs (e.g., Fanti 2009, Giroletti & Polatidis 2009). High-energy emission of the mini radio lobes have been theoretically explored by some authors (Stawarz et al. 2008; Kino et al. 2007, 2009). However, previous work has focused on leptonic processes and little is known about hadronic processes in the lobes.

In this Letter, we indicate that the hot spots in the mini radio lobe can be a plausible site of proton acceleration. Therefore, high energy protons are naturally expected in the mini lobes. In order to constrain the amount of high energy protons, next we examine the predicted photon spectra. Because of their smallness, observed mini radio lobes generally have dense synchrotron photon fields. Furthermore, the mini lobes are close to the AGN core and illuminated by the core emission. Therefore $p\gamma$ interaction is inevitable for the mini lobes. We calculate the photon spectra from the mini lobes taking into account the hadronic processes and show that the spectra are useful for constraining the amount of protons via γ-ray emission features. The predicted spectra will be useful for testing whether cosmic ray acceleration indeed takes place in mini lobes.

2 HADRONIC EMISSION

When a jet interacts with the surrounding medium, most of its kinetic energy is dissipated via shocks. The termination point of the jet is known as a hot spot and it is identified as the reverse shocked region. The shocked jet plasma escapes sideways from the spots forming a pair of radio lobes. Therefore, radio lobes are remnants of the decelerated jets which contain relativistic particles (e.g., Begelman et al. 1984). As for a ratio of electrons to protons in AGN jets, it is still under debate (e.g., Kino and Takahara (2004), Birzan et al. (2008)). There are case studies indicating that protons are dynamically dominant at hot spots of radio galaxies (e.g., Stawarz et al. 2007). Here we examine what happens when assuming the lobe contains relativistic protons. The notation $Q = Q_x \times 10^x$ is used unless otherwise noted.

2.1 Proton acceleration at the hot spots

Hot spots in powerful radio galaxies are one of the most promising sites for proton acceleration (e.g., Rachen and Biermann 1993). Here we show that hot spots in mini lobes are also possible sights for proton acceleration. The energy of shock accelerated protons is given by $\varepsilon_p = \gamma_p m_p c^2$ where γ_p is the proton Lorentz factor measured in the shock frame. Although a Bohm-type diffusion timescale is a rough approximation, we adopt it for simplicity. Then the acceleration timescale at the hot spot $t_{p,\rm acc,hs} = \xi_p \varepsilon_p/(eB_{\rm hs}c)$ in the case of relativistic shocks can be estimated as

$$t_{p,\rm acc,hs} \approx 3.5\ \varepsilon_{p,18} B_{\rm hs,-1}^{-1} \xi_{p,2}\ \rm yr, \tag{1}$$

where $B_{\rm hs}$, and ξ_p are the magnetic field strength, and the Gyro-factor for proton accelerations at the hot spot, respectively. Although there is no direct estimate of $B_{\rm hs}$, magnetic field strength in mini lobes ($B_{\rm lobe}$) has recently been estimated as $B_{\rm lobe} \sim 10 - 100$ mG by VLBI observations (Orienti & Dallacasa 2008). Since the magnetic field strength at the hot spot $B_{\rm hs}$ should be comparable to or larger than $B_{\rm lobe}$, here we set $B_{\rm hs} \sim 100$ mG. The value of ξ_p is a free parameter. In the case of blazars, ξ_p is not expected to be smaller than 10 (Inoue and Takahara 1996). As for mini lobes, there is little constraint on ξ_p. As a first step, we only treat the case of $\xi_p = 10^2$ in this Letter. The case of $\xi_p < 10^2$ is not observationally excluded and it is worth to examine it in the context of highest energy cosmic ray sources. When $\xi_p \gg 10^2$, photo-pion cascade does not occur. So, we do not treat it. The timescale of proton synchrotron cooling is

$$t_{p,\rm syn,hs} = \frac{6\pi m_p^4 c^3}{\sigma_T m_e^2 \varepsilon_p B_{\rm hs}^2} \approx 1.4\times10^4\ \varepsilon_{p,18}^{-1} B_{\rm hs,-1}^{-2}\ \rm yr, \tag{2}$$

where $\sigma_{\rm T}$ is the Thomson cross section. The escape velocity of shocked matter from the hot spot via sideways expansions is typically $v_{\rm esc,hs} \approx 0.3\ c$ (e.g., Kino and Takahara 2004). Then the escape timescale is $t_{\rm esc,hs} \approx 3\ R_{\rm hs,18}$ years where $R_{\rm hs}$ is the hot spot radius. Since $t_{\rm esc,hs} \ll t_{\rm syn,hs}$ is satisfied, the maximum energy of protons $\varepsilon_{p,\rm max}$ is obtained by the relation $t_{p,\rm acc,hs} = t_{\rm esc,hs}$ and it is

$$\varepsilon_{p,\rm max} \approx 0.9\times10^{18} B_{\rm hs,-1} R_{\rm hs,18} \xi_{p,2}^{-1}\ \rm eV. \tag{3}$$

The Larmor radius of protons in the spot ($r_{\rm L,hs}$) satisfies $R_{\rm hs} > r_{\rm L,hs} \approx 1\times10^{-2}\ \varepsilon_{p,18} B_{\rm hs,-1}^{-1}$ pc. Thus we find that the hot spots in mini lobes are feasible sites for proton acceleration. The escaped protons from the spots are then injected into the mini lobes and subsequently undergo cooling there.

2.2 Proton cooling in the mini radio lobes

The relativistic protons injected in mini lobes undergo various coolings. Before we describe the results of the Monte Carlo simulation in detail, it is worth estimating the relevant cooling timescales. First, the adiabatic loss timescale at the mini lobes is given by $t_{\rm ad} \approx 65\ (R_{\rm lobe}/2\ \rm pc)(v_{\rm exp,lobe}/0.1c)^{-1}$ yrs where $R_{\rm lobe}$ and $v_{\rm exp,lobe}$ are the radius and expansion velocity of the lobe, respectively. As shown above, the Larmor radius of protons of 10^{18} eV is sufficiently smaller than $R_{\rm lobe}$. Therefore, they are confined in the lobes and suffer adiabatic expansion loss. Next, we estimate the timescale of the photo-meson loss process of high energy protons. As shown in the introduction, $p\gamma$ interactions are expected in the lobe where target photons are UV photons from the accretion disk and synchrotron photons emitted by the lobe itself. The condition to create pions is $\varepsilon_p \varepsilon_{\gamma,i} \geqslant 0.2\ \rm GeV^2$ where $\varepsilon_{\gamma,i}$ is the target photon energy ($i = \rm disk, syn$). Then, the typical energy of protons interacting with the accretion disk photons is given by $\varepsilon_p \approx 2\times10^{16} (\varepsilon_{\gamma,\rm disk}/10\ \rm eV)^{-1}$ eV. The timescale of the $p\gamma$ interaction is $t_{p\gamma} \approx (n_{\gamma,i}\sigma_{p\gamma}c)^{-1} \approx 1.2\times10^4\ (LS/10\ \rm pc)^{-2} L_{\rm disk,45} (\varepsilon_{\gamma,\rm disk}/10\ \rm eV)^{-1}$ yr where $\sigma_{p\gamma} \approx 5\times10^{-28}\ \rm cm^{-2}$ at the resonance peak (Waxman and Bahcall 1997) and $L_{\rm disk}$ and $n_{\gamma,\rm disk}$ are the disk luminosity and the photon number density $n_{\gamma,\rm disk} \approx L_{\rm disk}/(4\pi LS^2 c\varepsilon_{\gamma,\rm disk})$, respectively. For $L_{\rm disk}$, we assume a value of observed big blue bumps in Seyfert 2 galaxies (e.g., Koratkar and Blaes 1999). In this case, we have $t_{\rm ad}/t_{p\gamma} \approx 5.3\times10^{-3} R_{\rm lobe} LS^2 L_{\rm disk}^{-1} \propto R_{\rm lobe}^3$ when we assume $LS \propto R_{\rm lobe}$. For protons with $\varepsilon_p > 2\times10^{16}$ eV, the target photons are the electron synchrotron ones. In this range, $n_{\gamma,\rm syn} \approx L_{\rm syn}/(\pi R_{\rm lobe}^2 c\varepsilon_{\gamma,\rm syn}) \approx 1.7\times10^4\ L_{\rm syn,44} (R_{\rm lobe}/2\ \rm pc)^{-2} (\varepsilon_{\gamma,\rm syn}/10^{-6}\ \rm eV)^{-1}\ cm^{-3}$ where $L_{\rm syn}$ is the synchrotron luminosity emitted by primary electrons. Then we have $t_{\rm ad}/t_{p\gamma} \approx 5.3\times10^{-4}\ R_{\rm lobe}^3 L_{\rm syn,44}^{-1} (\varepsilon_{\gamma,\rm syn}/10^{-6}\ \rm eV)^{-1} \propto R_{\rm lobe}^3$. So, $t_{p\gamma}$ become shorter than $t_{\rm ad}$ when $R_{\rm lobe}$ is sufficiently small, although such a case is beyond the scope of this work. The timescale of proton synchrotron loss at the lobe has been already given by Eq. (2) since we assume $B_{\rm lobe} \approx B_{\rm hs}$ for simplicity.

The timescale of energy loss by proton-proton collisions is given by $t_{pp} \sim 5\times10^7 (n_{\rm ext}/1\ \rm cm^{-3})^{-1}$ yr (Sikora et al. 1987) where $n_{\rm ext}$ is the number density of the ambient matter. Here we focus on the case of $t_{pp} \gg t_{\rm age} \sim 10^{2-3}$ yr. However, there is a possibility that mini lobes expand in rather dense environments involving clouds of gas emitting narrow emission lines with $n_{\rm ext} \gg 1\ \rm cm^{-3}$, and that $t_{pp} \sim t_{\rm age}$ holds. We will examine it in our future work.

3 RESULTANT SPECTRA

To calculate broadband photon spectra, the Monte Carlo simulation has been performed in this work. The details of numerical code have been described in Asano et al. (2007, 2008, 2009) and references therein. Here we briefly review the code. We calculate steady state spectra of protons ($i = p$) and electrons ($i = e$) by solving the following kinetic equations

$$q_i(\varepsilon_i) = -\frac{\partial}{\partial\varepsilon_i}\left[n_i(\varepsilon_i)\dot{\varepsilon}_i\right] + \frac{n_i(\varepsilon_i)}{t_{\rm ad}}, \tag{4}$$

where $n_i(\varepsilon_i)$, $\dot{\varepsilon}_i$, and $q_i(\varepsilon_i) = K_i \varepsilon_i^{-s_i} \exp\left(\frac{\varepsilon_i}{\varepsilon_{i,\rm max}}\right)$ for $\varepsilon_{i,\rm min} \leqslant \varepsilon_i$ are the number density, the cooling rate, and the injection rate of relativistic particles, respectively. Distributions of particles and photons are assumed to be isotropic. We assume that the common Fermi acceleration process works both for electrons and protons. In this case, the response to magnetic turbulences is same for relativistic particles with a same energy. Therefore, it is conservative to set $s_e = s_p$ and $\xi_e = \xi_p$. As explained in 2.1, $\varepsilon_{p,\rm max}$ are uniquely determined for given hot spot parameters. The maximum energy of electrons can be obtained as $\varepsilon_{e,\rm max} \sim 10\ B_{\rm hs,-1}^{-1/2} \xi_{e,2}^{-1/2}$ TeV from the relation $t_{e,\rm syn,hs} = t_{e,\rm acc,hs}$

where $t_{e,\rm syn,hs}$ and $t_{e,\rm acc,hs} = (\xi_e \varepsilon_e)/eB_{\rm hs}c$ are the synchrotron cooling and acceleration timescales for electrons, respectively. The kinetic equation of photons with the energy ε_γ is given by

$$\frac{\dot{N}_\gamma(\varepsilon_\gamma)}{\pi R_{\rm lobe}^2 c} = n_\gamma(\varepsilon_\gamma), \tag{5}$$

where $\dot{N}_\gamma(\varepsilon_\gamma)$ is the total production rate of each population of photons and $n_\gamma(\varepsilon_\gamma)$ is the corresponding photon number density. As for $\dot{N}_\gamma$ and $\dot{\gamma}_p$, we include the following physical processes: (1) photo-pion production from protons and neutrons ($p+\gamma \to p/n+\pi^0/\pi^+$), (2) the pions decay ($\pi^0 \to 2\gamma$) and ($\pi^+ \to \mu^+ + \nu_\mu \to e^+ + \nu_e + \nu_\mu + \bar{\nu}_\mu$), (3) photon-photon pair production ($\gamma + \gamma \to e^+ + e^-$), (4) Bethe-Heitler pair production ($p + \gamma \to p + e^+ + e^-$), (5) synchrotron and inverse Compton processes from electrons/positrons, protons, pions, muons with Klein-Nishina cross section, and (6) synchrotron self-absorption for electrons/positrons.

The model parameter values are summarized here. For the hot spot, we set $R_{\rm hs} = 0.3$ pc, $B_{\rm hs} = 0.1$ G, and $v_{\rm esc,hs} = c/3$. These hot spot quantities uniquely determine $\varepsilon_{i,\rm max}$. We adopt $\xi_p = \xi_e = 1 \times 10^2$, $s_p = s_e = 2$, and $\varepsilon_{p,\rm min}/m_p c^2 = \varepsilon_{e,\rm min}/m_e c^2 = 10$ for particle injections. The mini lobes parameters are $R_{\rm lobe} = 2$ pc, $B_{\rm lobe} = 0.1$ G, $v_{\rm exp,lobe} = 0.1\,c$, and $LS = 10$ pc. The accretion disk quantities are assumed as $L_{\rm disk} = 3 \times 10^{45}$ erg s^{-1} with the average temperature 10 eV. Because of the obscuration by surrounding dusty torus $L_{\rm disk}$ in mini radio lobes is not directly constrained. Following the work of Ostorero et al. (2010), here we assume $L_{\rm disk}$ as the same one in luminous blazars. The injection power of protons L_p should be smaller than the total kinetic powers of powerful jets $\sim 10^{47-48}$ erg s^{-1} (e.g., Ito et al. 2008, Ghisellini et al. 2009). Here $L_p = 5 \times 10^{46}$ erg s^{-1} is assumed. Various injection powers of electrons L_e will be examined below.

3.1 Leptonic-hadronic model

Fig. 1 displays the resultant photon spectrum for $L_e = 1 \times 10^{42}$ erg s^{-1} (the thick solid line). There are several distinct features in the spectrum.

(i) The bump at $\sim$ sub PeV energies is composed of π^0-decay photons. The $\gamma\gamma$ absorption opacity against the target photons with the energy $\varepsilon_{\gamma,\rm tgt}$ at the threshold $\varepsilon_\gamma \varepsilon_{\gamma,\rm tgt} \sim (2m_e c^2)^2$ is written as $\tau_{\gamma\gamma}(\varepsilon_\gamma) = (3/8)\sigma_{\rm T} n_{\gamma,\rm tgt} R_{\rm lobe}$ (e.g., Razzaque et al. 2004) and it is estimated as

$$\tau_{\gamma\gamma}(\varepsilon_\gamma = 10^{14}\ {\rm eV}) \approx 0.8\ \frac{L_{\gamma,\rm tgt}}{3\times10^{40}\ {\rm erg\ s^{-1}}}\frac{R_{\rm lobe}}{2\ {\rm pc}} \times \left(\frac{\varepsilon_{\gamma,\rm tgt}}{10^{-2}\ {\rm eV}}\right)^{-1} \tag{6}$$

where the number density of target photons is $n_{\gamma,\rm tgt} = \dot{N}_{\gamma,\rm tgt}/(\pi R_{\rm lobe}^2 c) = L_{\gamma,\rm tgt}/(\pi \varepsilon_{\gamma,\rm tgt} R_{\rm lobe}^2 c)$. Hence, the π^0-decay photons with $\varepsilon_\gamma \sim 10^{14}$ eV can partially escape from the lobe. The escaped 100 TeV photons, however, would be absorbed by the radio background photons during their propagations since their mean free path is shorter than 10 Mpc (e.g., Coppi and Aharonian 1997).

(ii) The secondary electrons/positrons produce the synchrotron bump at $\sim$ GeV. They are produced via μ- and π-decays. The $e^\pm$ pairs created by the $\gamma\gamma$ absorption of the $\pi^0 \to 2\gamma$ photons have an energy of $1/2 \times 1/2 = 1/4$ that of the parent π^0. In the π^+ decay mode, the comparable fraction of the energy is converted from the parent π^+ to the positron. Then, the synchrotron emission from secondary electrons/positrons with $\sim 10^{15}$ eV has its peak at $\sim$ GeV.

(iii) The proton synchrotron bump (p-SYN) appears at MeV energy band with the peak at $\nu_{p,\rm syn} \approx (\varepsilon_p^2 e B_{\rm lobe}/2\pi m_p^3 c^5) \approx 0.7\ \varepsilon_{p,18}^2 B_{\rm lobe,-1}$ MeV. Below $\sim$ keV, the synchrotron emission from the primary electrons overwhelms the proton synchrotron emission. Protons also transfer energy to photons by inverse Compton scattering and the photon spectrum is shown in the thin line (p-IC). However, they do not escape from the lobe because of the $\gamma\gamma$ absorption.

(iv) The break of synchrotron spectrum at $\sim$ GHz is well known synchrotron self absorption (SSA) observed by VLBI observations (e.g., Snellen et al. 2000). The SSA turnover frequency for $s_e = 2$ is given by $\nu_{\rm ssa} \sim 0.39\ B_{\rm lobe,-1}^{1/7} \left(\frac{L_{\rm ssa}}{10^{41}\ {\rm erg\ s^{-1}}}\right)^{2/7} \left(\frac{R_{\rm lobe}}{2\ {\rm pc}}\right)^{-4/7}$ GHz (Kellermann and Pauliny-Toth 1981) where $L_{\rm syn} > L_{\rm ssa} \equiv \nu_{\rm ssa} L_{\nu_{\rm ssa}}$. The electrons with $\gamma_e \sim 100$ emitting synchrotron at $\sim$ 1 GHz will cool down, since the synchrotron cooling timescale satisfies $t_{e,\rm syn} \sim 25\ B_{\rm lobe,-1}(\gamma_e/10^2)^2 {\rm yr} < t_{\rm ad}$. Therefore the cooling break frequency obtained from $t_{e,\rm syn} = t_{\rm ad}$ is comparable to or below $\nu_{\rm ssa}$. This implies that $L_e \approx L_{\rm syn}$.

(v) For comparison, the case of no-proton injection (i.e., $L_p = 0$) is shown in the thin solid line. By comparing the spectrum to the one with proton injection, we can clearly recognize the contribution of the hadronic emission in the γ-ray energy domain.

Fig. 2 shows the photon spectra for $L_e = 1 \times 10^{45}$ erg s^{-1}, 1×10^{44} erg s^{-1}, 1×10^{43} erg s^{-1}, 1×10^{42} erg s^{-1}, and 1×10^{41} erg s^{-1}. The L_p/L_e ratio in AGN jets is not well known. The examined L_p/L_e ratio here partly exceeds the ratio of $\sim 10^2$ measured around the Earth. However, when a jet with $L_p/L_e \sim 10^2$ gradually decreases its power keeping the L_p/L_e ratio, the resultant spectrum may be similar to the one for larger L_p/L_e because of fast cooling of electrons. The spectra with and without proton injection are displayed with thick and thin solid lines, respectively. For $L_e = 1 \times 10^{45}$ erg s^{-1}, the leptonic emissions overwhelm hadronic ones at all energy domains. As L_e decreases to $L_e \leqslant 1 \times 10^{44}$ erg s^{-1}, thick and thin lines become separable in the γ-ray domain because the synchrotron emission from the secondary electrons/positrons overwhelms the inverse Compton component from primary accelerated electrons. In MeV range, the proton synchrotron bump appears for smaller L_e. Typical $L_{\rm syn}$ depends on the source population. CORALZs typically have $L_{\rm ssa} \sim 10^{40-42}$ erg s^{-1} while HFPs have $L_{\rm ssa} \sim 10^{44-46}$ erg s^{-1}. Observed turnover frequencies of mini lobes shows $\nu_{\rm ssa} \sim 0.1 - 10$ GHz. The maximum $\nu_{\rm ssa}$ in Fig. 2 is smaller than the ones for HFPs, mainly because the angular size of the lobe in our model is larger by a factor of a few than the one for HFPs. It does not affect the main results of this work. The synchrotron self Compton component appeared in γ-ray bands is less dominant than the synchrotron one since $U_{\rm syn} \leqslant B_{\rm lobe}^2/8\pi \approx 4 \times 10^{-4} B_{\rm lobe,-1}^2$ erg cm^{-3} holds for $L_{\rm syn} < 10^{45}$ erg s^{-1} where $U_{\rm syn}$ is the energy density of synchrotron photons.

When $L_e < 10^{44}$ erg s^{-1}, the TeV photons in the lobe be-

come transparent against $\gamma\gamma$ absorption because of $\tau_{\gamma\gamma}(\varepsilon_\gamma = 10^{12}\ \mathrm{eV}) \sim 0.8(L_{\gamma,\mathrm{tgt}}/3\times10^{42}\ \mathrm{erg\ s^{-1}})(\varepsilon_{\gamma,\mathrm{tgt}}/1\ \mathrm{eV})$. Then the TeV photons begin to escape from the lobe.

3.2 Pure hadronic model

In Fig. 3, we show the spectrum with the same parameters as Fig. 1 but for pure proton injection (i.e., $L_e = 0$) with the proton injection duration $t_{\rm inj} = 90$ yrs. In order to realize $L_e = 0$ approximation, $t_{\rm inj} < t_{\rm age}$ and $t_{e,\rm syn} < t_{\rm age}$ should be satisfied where $t_{e,\rm syn}$ is the synchrotron cooling timescale for electrons. In this case, the injection has been already stopped and primary electrons have been already cooled down. Since the source age in this model can be estimated as $t_{\rm age} \sim LS/v_{\rm exp} \sim 3\times10^2$ yr and it agrees with the observational estimates of $t_{\rm age} \sim 10^{2-3}$ yr (e.g., Giroletti 2009), the conditions of $t_{\rm inj} < t_{\rm age}$ and $t_{\rm age} > t_{e,\rm syn} \sim 25\ B_{\rm lobe,-1}(\gamma_e/10^2)^2$ yr are indeed justified. The model considered here is not applicable when B satisfy $t_{\rm age} < t_{e,\rm syn}$. Short $t_{\rm inj}$ would be naturally realized for jets with intermittent activities. For example, the recurrent mini lobe 3C 84 actually show $t_{\rm inj} \sim 50$ yr (Asada et al. 2006). The low power mini lobes which seem to be dying ones (Giroletti et al. 2005) could also be candidates. In this model, the deposited energy of protons is given by $L_p t_{\rm inj}$.

The prominent three bumps of hadronic emissions, i.e., the π^0-decay photon bump at $\sim$ PeV, the synchrotron one from secondary electrons/positrons at $\sim$ GeV, and the proton synchrotron one at $\sim$ MeV, which have also been predicted in Fig. 1 emerge more clearly. The escaped PeV photons from the lobe are absorbed by the radio background photons and they may not reach the Earth.

Below the optical energy band, the synchrotron emission from secondary $e^\pm$ pairs via Bethe-Heitler process ($p\gamma \to pe^-e^+$) is responsible for the emission. The protons with $\varepsilon_p \sim 10^{14}$ eV interact with the disk photons and convert a fraction of $\sim m_e/m_p$ of their energy to create $e^\pm$ pairs. Then the pairs with $\sim 10^{11}$ eV radiate synchrotron emission peaked at $\sim$ optical band. Since the lobes are dim in radio band, we may call them radio-dark γ-ray lobes.

4 SUMMARY AND DISCUSSION

In this work, we point out that the hot spots in mini lobes are feasible sites of proton acceleration. Next, the expected photon spectra of the mini lobes including the hadronic processes are explored. Summary and discussions are as follows.

(i) For bright lobes with $L_e \sim L_{\rm syn} \sim 10^{45}\ \mathrm{erg\ s^{-1}}$, the predicted high energy emission is detectable with the current γ-ray telescopes. However, it is overwhelmed by the leptonic inverse Compton component, and it seems hard to test whether the emission is of hadronic- or leptonic-origin. For $L_e \sim L_{\rm syn} \leqslant 10^{43}\ \mathrm{erg\ s^{-1}}$, proton synchrotron bump appears at $\sim$ MeV and the synchrotron emission from the secondary electrons/positrons generated by the μ- and π-decays emerges at $\sim$ GeV. The two distinctive bumps in γ-ray domain are of hadronic origin.

(ii) The case of the short term particle injection is examined. It may be realized when jets have intermittent activities. Typically, primary accelerated electrons have been cooled down but protons have not. Then, the predicted emission is purely hadronic and the hadronic bumps are clearly seen. Importantly, the high energy tail of the GeV bump is detectable by *The Cherenkov Telescope Array (CTA)* (http://www.cta-observatory.org/). These sources may be identified as radio dark γ-ray lobes.

(iii) The predicted X-ray flux is well above the detection limit of *XMM*. The observations actually show bright *X*-ray emission. This is traditionally interpreted as thermal radiation from the accretion disk and the possibility of lobe emission has been alternatively indicated (Ostorero et al. 2010 and reference therein). In any case, X-ray emission is likely composed of various different components. Therefore, it seems difficult to extract the hadronic component from the X-ray band.

(iv) We comment on the importance of larger $n_{\rm ext}$ it may lead to frre-free absorption (FFA) in radio band (e.g., Begelman 1999; Bicknell 2003; Stawarz et al. 2008). Actually, the low frequency turnover in the radio spectra of some sources are indeed reproduced by FFA and not by SSA (e.g., OQ 208, Kameno et al. 2000; 0108+388, Marr et al. 2001). It is clear that dense emvironments lead to an effective proton-proton collision. We will examine it in the future.

(v) We add a comment on the recent VLBI observation of mini lobe 3C 84. It shows the outburst around 2005 and a new component smaller than 1 pc emerges (Nagai et al. 2010). Fermi/LAT also detect GeV γ-ray emission from it (Abdo et al. 2009). A future collaboration with Space VLBI project VSOP-2 with high angular resolution (http://www.vsop.isas.jaxa.jp/vsop2/) and *CTA* would provide us valuable constraints on the hadronic model. Theoretically, we plan to conduct studies with smaller $R_{\rm lobe}$ in our future work.

ACKNOWLEDGMENTS

We thank the referee for comments to improve this paper. We are indebted to H. Takami, H. Nagai, M. Orienti and N. Kawakatu for useful comments and discussions.

REFERENCES

Abdo A. A., et al., 2009, ApJ, 699, 31
Asada K., Kameno S., Shen Z.-Q., Horiuchi S., Gabuzda D. C., Inoue M., 2006, PASJ, 58, 261
Asano K., Guiriec S., Mészáros P., 2009, ApJ, 705, L191
Asano K., Mészáros P., 2008, ApJ, 677, L31
Asano K., Inoue S., 2007, ApJ, 671, 645
Begelman M. C., Blandford R. D., Rees M. J., 1984, RvMP, 56, 255
Begelman M. C., 1999, in The Most Distant Radio Galaxies, ed. H. J. A. Rottgering, P. N. Best, and M. D. Lehnert, Royal Netherlands Academy of Arts and Sciences, 173
Bicknell G. V., Saxton C. J., Sutherland R. S., 2003, PASA, 20, 102
Bîrzan L., McNamara B. R., Nulsen P. E. J., Carilli C. L., Wise M. W., 2008, ApJ, 686, 859
Coppi P. S., Aharonian F. A., 1997, ApJ, 487, L9
de Vries N., Snellen I. A. G., Schilizzi R. T., Mack K.-H., Kaiser C. R., 2009, A&A, 498, 641
Fanti C., Fanti R., Dallacasa D., Schilizzi R.T., et al. 1995, A&A, 302, 317

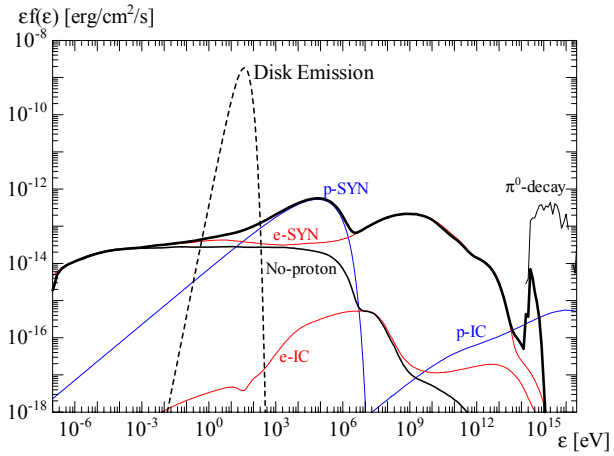

Figure 1. Predicted photon spectrum from the mini radio lobe for $L_e = 1 \times 10^{42}$ erg s^{-1}, $L_p = 5 \times 10^{46}$ erg s^{-1} and $L_{\rm disk} = 3 \times 10^{45}$ erg s^{-1}. The thick solid line represents the spectrum including the effect of internal $\gamma\gamma$ absorption. Thin blue lines show the proton emissions, while thin red lines represent electron emissions before including the $\gamma\gamma$ absorption. The luminosity is converted to the flux with the distance 100 Mpc.

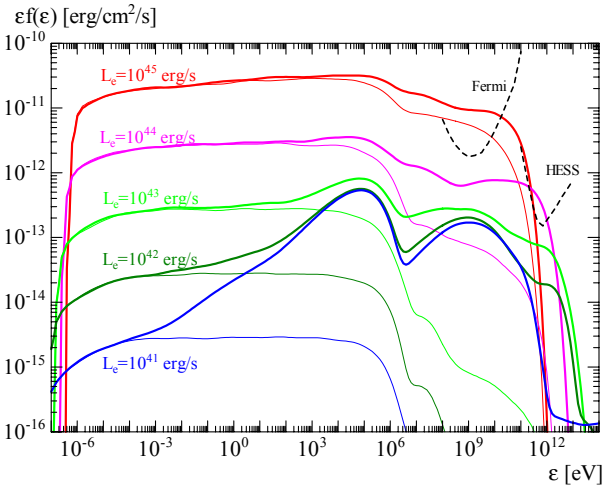

Figure 2. Same as Fig. 1 but for various $L_{\rm e}$ from $L_{\rm e} = 1 \times 10^{45}$ erg s^{-1} to 1×10^{41} erg s^{-1}. The sensitivities of *Fermi*/LAT, and HESS are, respectively, the ones for 1 year, and 50 h integration time.

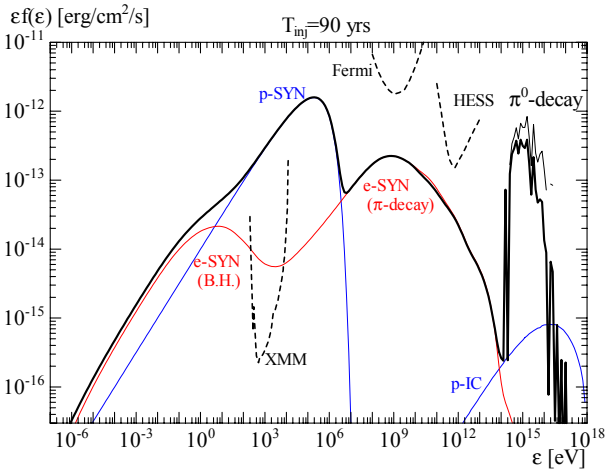

Figure 3. Same as Fig. 1 but for the case pure proton injection $t_{\rm inj} = 90$ years. The synchrotron emission from electrons/protons produced via Bethe-Heitler process and pion- and muon-decay are predicted. The Proton synchrotron peaks at $\sim$ MeV. PeV photons via pion-decay are absorbed during their propagations. The sensitivity for *XMM-Newton* is normalized by 100 ks integration time.

Fanti C., 2009, AN, 330, 120
Ghisellini G., Tavecchio F., Ghirlanda, G. 2009, MNRAS, 399, 2041
Giroletti M., Polatidis A., 2009, AN, 330, 193
Giroletti M., Giovannini G., Taylor G. B., 2005, A&A, 441, 89
Inoue S., Takahara F., 1996, ApJ, 463, 555
Ito H., Kino M., Kawakatu N., Isobe N., Yamada S., 2008, ApJ, 685, 828
Kameno S., Horiuchi S., Shen Z.-Q., Inoue M., Kobayashi H., Hirabayashi H., Murata Y., 2000, PASJ, 52, 209
Kino M., Ito H., Kawakatu N., Nagai H., 2009, MNRAS, 395, L43
Kino M., Kawakatu N., Ito H., 2007, MNRAS, 376, 1630
Kino M., Takahara F., 2004, MNRAS, 349, 336
Kellermann K. I., Pauliny-Toth I. I. K., 1981, ARA&A, 19, 373
Koratkar A., Blaes O., 1999, PASP, 111, 1
Marr J. M., Taylor G. B., Crawford F., III, 2001, ApJ, 550, 160
Nagai H., et al., 2010, PASJ, 62, L11
O'Dea C. P., Baum S. A., 1997, AJ, 113, 148
Orienti M., Dallacasa D., Stanghellini C. 2007, A&A, 475, 813
Orienti M., Dallacasa D., 2008, A&A, 487, 885
Ostorero L., et al., 2010, ApJ, 715, 1071
Rachen J. P., Biermann P. L., 1993, A&A, 272, 161
Razzaque S., Mészáros P., Zhang B., 2004, ApJ, 613, 1072
Readhead A. C. S., Taylor G. B., Pearson T. J., Wilkinson P. N., 1996, ApJ, 460, 612
Sikora M., Kirk J. G., Begelman M. C., Schneider P., 1987, ApJ, 320, L81
Snellen I. A. G., Mack K.-H., Schilizzi R. T., Tschager W., 2004, MNRAS, 348, 227
Snellen I.A.G., Schilizzi R.T., Miley G.K. et al. 2000, MNRAS, 319, 445
Stawarz Ł., Cheung C. C., Harris D. E., Ostrowski M., 2007, ApJ, 662, 213
Stawarz Ł., Ostorero L., Begelman M. C., Moderski R., Kataoka J., Wagner S., 2008, ApJ, 680, 911
Walker R. C., Dhawan V., Romney J. D., Kellermann K. I., Vermeulen R. C., 2000, ApJ, 530, 233
Waxman E., Bahcall J., 1997, PhRvL, 78, 2292